Turk Neurosurg, 2024

Original Investigation

Received: 15.09.2023
Accepted: 15.01.2024

DOI: 10.5137/1019-5149.JTN.45482-23.2

Published Online: 23.10.2024

Analysis of the Cranial Aperture of the Optic Canal in Patients with Chiari Type-I Malformation

Hakan OZALP[1], Onur OZGURAL[2], Baran Can ALPERGIN[2], Aysenur INCEOGLU[3], Sibel OZALP[4], Ercan ARMAGAN[5], Hadice UCAR[3], Orhan BEGER[3]

[1]Istanbul Medipol University Faculty of Medicine, Department of Neurosurgery, Istanbul, Türkiye
[2]Ankara University Faculty of Medicine, Department of Neurosurgery, Ankara, Türkiye
[3]Gaziantep University Faculty of Medicine, Department of Anatomy, Gaziantep, Türkiye
[4]Istanbul Medipol University School of Vocation, Department of Medical Laboratory Techniques, Istanbul, Türkiye
[5]Silivri Anadolu Hospital, Department of Neurosurgery, Istanbul, Türkiye

Corresponding author: Baran Can ALPERGIN ✉ balpergin@gmail.com

ABSTRACT

AIM: To examine the morphological properties of the cranial aperture of the optic canal (CAOC) in patients with a Chiari type-I malformation (CIM).

MATERIAL and METHODS: Radiological images of 40 patients with CIM (24 females/16 males, mean age: 20.75 ± 14.98 years) and 40 normal individuals (24 females/16 males, mean age: 23.13 ± 18.89 years) were included in the study to assess the anatomical features of CAOC.

RESULTS: The CAOC width (p=0.137), CAOC height (p=0.243), distance between the CAOC and the midsagittal line (p=0.982), and angle of the optic canal in the sagittal plane (Ang-in-SP) (p=0.598) were similar in patients with CIM and in the controls. The distances between the CAOC and the anterior (Dis-to-AB) and lateral (Dis-to-LB) boundaries of the anterior skull base were smaller in patients with CIM than in the controls (p<0.01). However, the angle of the optic canal in the axial plane (Ang-in-AP) was greater in patients with CIM than in the controls. Four different aperture shapes were identified in the CIM group (teardrop, n=42 [52.40%]; triangular, n=17 [21.30%]; oval, n=9 [11.30%]; and round, n=12 [15%]) and in the control group (teardrop, n=36 [45%]; triangular, n=14 [17.50%]; oval, n=10 [12.50%]; and round, n=20 [25%]).

CONCLUSION: A greater Ang-in-AP and shorter Dis-to-LB and Dis-to-AB were found in patients with CIM than in the healthy controls. The distance measurements demonstrate that patients with CIM have a shorter and narrower anterior fossa than normal individuals.

KEYWORDS: Optic canal, Cranial aperture, Computed tomography, Chiari type-I malformation, Morphometric, Transcranial approaches

INTRODUCTION

The cranial aperture of the optic canal (CAOC) is a gateway between the middle fossa and the orbit that transmits the ophthalmic artery, optic nerve, and sympathetic fibers (2,32,55). These neurovascular structures may be affected by pathological entities, such as an anterior clinoidal meningioma, located around the CAOC (13,14,22,35,48,60,62). Histo-anatomical evaluations have demonstrated that optic nerve compression mostly occurs in the proximal part of the optic canal (22,40,62). This is due to isolated entities arising from the optic nerve and ophthalmic artery (e.g., optic meningioma) and large entities originating from the sellar region (e.g., tuberculum sellae meningioma) (13,22,35,40,48,56,61). Some surgeons consider removal of only the proximal portion of

Hakan OZALP : 0000-0002-8234-8013
Onur OZGURAL : 0000-0003-0592-6139
Baran Can ALPERGIN : 0000-0002-3575-0480
Aysenur INCEOGLU : 0000-0001-6988-1705
Sibel OZALP : 0000-0001-5627-1422
Ercan ARMAGAN : 0000-0001-8289-8667
Hadice UCAR : 0000-0001-6516-4071
Orhan BEGER : 0000-0002-4932-8758

the optic canal sufficient for optic canal decompression in some subjects (22,56,62). Thus, knowledge of the angulation, dimension, and depth of the proximal portion may be helpful in ensuring accurate intraoperative orientation during implant positioning (15). Therefore, detailed anatomical data related to the morphologic features of the optic canal's proximal portion, including the CAOC, are needed by neurosurgeons to perform a successful operation.

Some authors have reported substantial alterations in the anterior and middle fossae of patients with a Chiari type-I malformation (CIM) in addition to those in the posterior fossa, which may have occurred due to a mesodermal defect (39,52). For instance, patients with CIM have a longer anterior fossa than healthy individuals (52). Moreover, they have a 38% greater sphenoid sinus volume than the healthy individuals (9.3 ± 3.0 vs. 6.7 ± 1.9 cm^3) (39). Therefore, the increased sphenoid sinus volume may affect the angulation, dimension, and shape of the anatomical structures located around the sellar region (e.g., the pterygoid canal, prechiasmatic sulcus, sella turcica, and optic canal). Alterations in the anatomy of the optic canal's proximal portion, including the CAOC, may affect the intraoperative surgical orientation, positioning of the patient's head, and choice of surgical approach for preventing complications (e.g., vision loss and bleeding) (13,22,24,40,57,62). However, the existing studies, including shape evaluations, morphometric analyses, detailed anatomical definitions, and surgical procedure investigations, are mainly conducted in healthy individuals. Herein, we have aimed to use computed tomography (CT) to determine whether the CAOC morphology is altered in CIM or not when compared with normal individuals.

MATERIAL and METHODS

Study Population

This retrospective study was approved by the The Clinical Research Ethics Committee of Ankara University (confirmation no: 2023/169, date: 05/04/2023). The medical records of the study participants were retrospectively reviewed and the following data were collected: hospital admission/discharge dates, treatment procedures, diagnosis, complaints, cranial CT images, age at presentation, and sex. According to the criteria (Table I), the individuals were divided into the following two groups: patients with CIM and controls (an age- and sex-matched set).

CT Protocol

CT images of the patients' skull bases were obtained using a 64-row multidetector scanner (Aquillion 64, Toshiba Medical Systems, Tokyo, Japan). The CT parameters were as follows: matrix, 512 x 512; field of view, 240 mm; pixel size, 0.46 mm; slice thickness, 0.5 mm; tube current, 230 mA; tube voltage, 120 kV; and interval, 0.3 mm. By transferring the data to a workstation, the raw data were converted into three-dimensional (3D) images and reformatted in different planes (sagittal, coronal, and axial).

Measured Parameters

The selected parameters and their explanations for determining CAOC morphology are presented in Table II (57). The angle of the optic canal in the axial plane (Ang-in-AP), the distances between the CAOC and the anterior (Dis-to-AB) and lateral (Dis-to-LB) boundaries of the anterior skull, and the distance between the CAOC and the midsagittal line (Dis-to-MSL) were

Table I: The Inclusion and Exclusion Criteria for the Study Populations

Criteria	CIM	Control group
Inclusion criteria	patients with CIM	patients without malformations (syndromic or genetic)
	patients without a history of surgical intervention around the optic canal	patients without fractures, infections, tumors
	patients with good quality CT images	patients without a history of surgical intervention around the optic canal
		patients without a history of medical treatment related to the optic canal
		patients with good quality CT images
Exclusion criteria	patients with the other types of Chiari malformation	patients with malformations (syndromic or genetic)
	patients with a history of surgical intervention around the optic canal	patients with fractures, infections, tumors
	patients with low quality CT images	patients with a history of surgical intervention around the optic canal
		patients with a history of medical treatment related to the optic canal
		patients with low quality CT images

measured on the axial images. The CAOC height (CAOC-H) and CAOC width (CAOC-W) were measured on the coronal images. Additionally, the angle of the optic canal in the sagittal plane (Ang-in-SP) was measured on the sagittal images (Figures 1 and 2).

Shape of the CAOC

In previous studies (1,3,23,34,57), the following CAOC shapes have been identified: polygonal, rhomboidal, triangular, teardrop, round, elliptical, and oval (ovoid). We classified patients based on these shapes.

Statistical Analysis

Statistical evaluations were performed using SPSS (version 22.0; IBM, Armonk, NY, USA). CIM/control and male/female comparisons were performed using the Mann–Whitney U test. Right-sided/left-sided comparisons were performed using the Wilcoxon test. Dispersion of CAOC shapes in the controls and

Table II: Definations of the Parameters

Parameters	Descriptions
CAOC-H	the vertical diameter of CAOC in coronal plane on CT
CAOC-W	the horizontal diameter of CAOC in coronal plane on CT
Dis-to-AB	the distance between CAOC (the frontmost point) and the anterior boundary of the anterior skull base in axial plane on CT
Dis-to-LB	the distance between CAOC (the most lateral point) and the lateral boundary of the anterior skull base in axial plane on CT
Dis-to-MSL	the distance between CAOC (the most medial point) and the midsagittal line in axial plane on CT
Ang-in-AP	the angle between the optic canal and the sagittal horizontal line (i.e., the midline axis) in axial plane on CT
Ang-in-SP	the angle between the optic canal and the sagittal horizontal line (i.e., the line parallel to the ground) in sagittal plane on CT

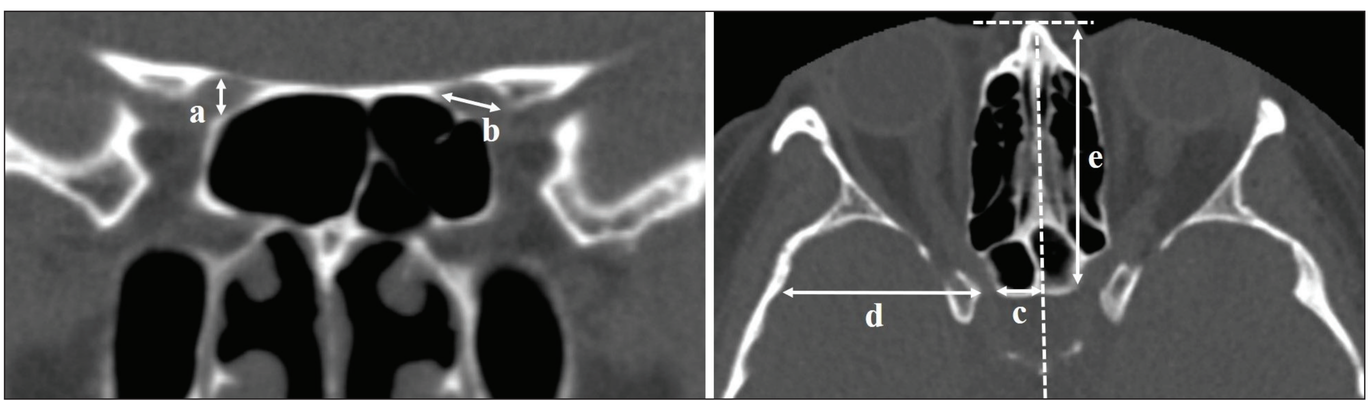

Figure 1: Parameters: **a)** CAOC-H, **b)** CAOC-W, **c)** Dis-to-MSL, **d)** Dis-to-LB, and **e)** Dis-to-AB.

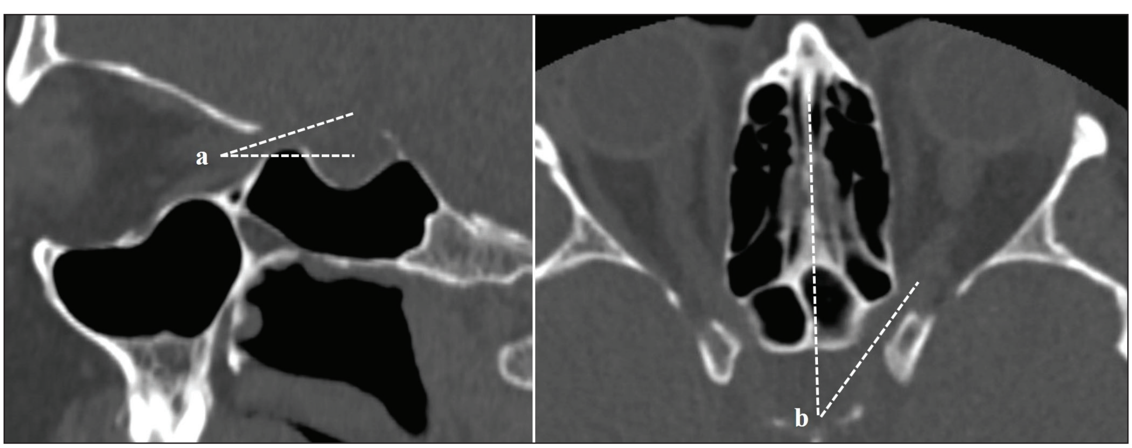

Figure 2: Parameters: **a)** Ang-in-SP and **b)** Ang-in-AP.

patients with CIM was evaluated using the chi-square test. The normality of the data was assessed using the Shapiro–Wilk test. A p-value of <0.05 was considered statistically significant.

RESULTS

Radiological images of 40 patients (24 females/16 males) with CIM, aged 20.75 ± 14.98 years, and admitted to the hospital between 2010 and 2022 were included in the study. Additionally, the radiological images of 40 healthy individuals (24 females/16 males), aged 23.13 ± 18.89 years, were also included in the study. Our findings are as follows:

- Compared with the controls, patients with CIM had a smaller Dis-to-LB (p=0.003) and Dis-to-AB (p<0.001) but greater Ang-in-AP (p=0.006). The Ang-in-SP (p=0.598), CAOC-H (p=0.243), CAOC-W (p=0.137) and Dis-to-MSL (p=0.982) were similar between the patients CIM and the controls (Table III).
- Among the patients with CIM, the males had a smaller Ang-in-SP than the females (p=0.037) (Table IV).
- Among the healthy controls, the males had a smaller Ang-in-SP (p=0.049) but greater Dis-to-AB (p=0.001) and Dis-to-MSL (p=0.002) than the females. Furthermore, the CAOC-H (p=0.001) and CAOC-W (p < 0.001) were smaller on the right side than on the left side (Table IV).
- Four different CAOC shapes were identified in the patients with CIM (teardrop, n=42 [52.40%]; triangular, n=17 [21.30%]; round, n=12 [15%]); and oval, n=9 [11.30%] and the healthy controls teardrop, n=36 [45%]; round, n=20 [25%]); triangular, n=14 [17.50%]; and oval, n=10 [12.50%]) (Figure 3).

Table III: Comparison of CM-I and the Control Group

Parameters	CIM (n=80)	Control (n=80)	p-value
CAOC-H (mm)	3.69 ± 0.69 (1.86-5.80)	3.75 ± 1.18 (1.99-7.28)	0.243
CAOC-W (mm)	5.15 ± 0.96 (2.82-7.59)	5.30 ± 1.25 (2.05-7.70)	0.137
Dis-to-AB (mm)	52.82 ± 6.14 (42.50-72)	57.41 ± 7.40 (36.60-74.10)	**<0.001**
Dis-to-LB (mm)	37.50 ± 4.21 (24.90-47.20)	39.43 ± 4.49 (23.60-48.20)	**0.003**
Dis-to-MSL (mm)	7.64 ± 1.64 (4.60-12.80)	7.67 ± 1.91 (3.23-11.80)	0.982
Ang-in-AP (°)	34.42 ± 5.29 (24.50-46)	31.80 ± 4.89 (19.60-42.20)	**0.006**
Ang-in-SP (°)	15.04 ± 3.80 (8.10-27.40)	14.97 ± 3.28 (6.20-24.10)	0.598

N: *Numbers of sides,* ***CAOC-H:*** *The vertical diameter of CAOC,* ***CAOC-W:*** *The horizontal diameter of CAOC,* ***Dis-to-AB:*** *The distance between CAOC (the frontmost point) and the anterior boundary of the anterior skull base,* ***Dis-to-LB:*** *The distance between CAOC (the most lateral point) and the lateral boundary of the anterior skull base,* ***Dis-to-MSL:*** *The distance between CAOC (the most medial point) and the midsagittal line,* ***Ang-in-AP:*** *The angle between the optic canal and the sagittal horizontal line in axial plane,* ***Ang-in-SP:*** *The angle between the optic canal and the sagittal horizontal line in sagittal plane.*

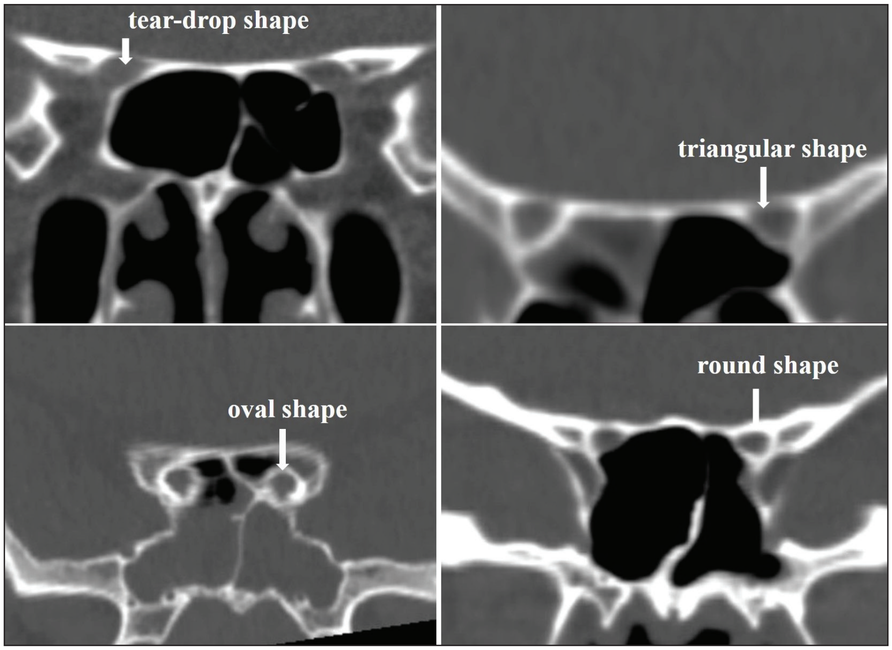

Figure 3: Aperture shapes on coronal CT images.

Table IV: Sex and Side Comparisons for CIM and the Control Group

	Parameters	Females (n=48)	Males (n=32)	p-value	Right (n=40)	Left (n=40)	p-value
CIM	CAOC-H (mm)	3.77 ± 0.64	3.58 ± 0.76	0.235	3.61 ± 0.65	3.78 ± 0.73	0.281
	CAOC-W (mm)	5.17 ± 0.87	5.13 ± 1.10	0.867	5.08 ± 0.95	5.23 ± 0.99	0.467
	Dis-to-AB (mm)	52.51 ± 5.53	53.25 ± 6.95	0.647	52.94 ± 6.18	52.71 ± 6.17	0.807
	Dis-to-LB (mm)	37.99 ± 3.68	36.80 ± 4.85	0.215	37.93 ± 4.43	37.07 ± 3.99	0.310
	Dis-to-MSL (mm)	7.89 ± 1.59	7.26 ± 1.66	0.080	7.64 ± 1.70	7.64 ± 1.59	0.996
	Ang-in-AP (°)	34.25 ± 4.77	34.68 ± 6.07	0.825	33.81 ± 4.99	35.03 ± 5.58	0.341
	Ang-in-SP (°)	15.83 ± 4.10	13.84 ± 2.98	**0.037**	15.18 ± 3.93	14.89 ± 3.71	0.791
	Parameters	**Females (n=48)**	**Males (n=32)**	**p-value**	**Right (n=40)**	**Left (n=40)**	**p-value**
Control	CAOC-H (mm)	3.49 ± 0.94	4.14 ± 1.39	0.147	3.24 ± 0.54	4.26 ± 1.41	**0.001**
	CAOC-W (mm)	5.37 ± 1.15	5.19 ± 1.40	0.404	4.71 ± 1.29	5.89 ± 0.89	**<0.001**
	Dis-to-AB (mm)	55.55 ± 7.44	60.19 ± 6.52	**0.001**	57.59 ± 7.56	57.23 ± 7.34	0.862
	Dis-to-LB (mm)	38.83 ± 5.01	40.35 ± 3.47	0.116	39.46 ± 4.55	39.41 ± 4.49	0.988
	Dis-to-MSL (mm)	7.10 ± 1.68	8.53 ± 1.94	**0.002**	7.50 ± 1.77	7.84 ± 2.05	0.593
	Ang-in-AP (°)	30.97 ± 4.99	33.03 ± 4.53	0.088	31.87 ± 4.76	31.72 ± 5.07	0.881
	Ang-in-SP (°)	15.64 ± 3.08	13.97 ± 3.36	**0.049**	14.90 ± 3.32	15.05 ± 3.28	0.935

n: *Numbers of sides,* ***CAOC-H:*** *The vertical diameter of CAOC,* ***CAOC-W:*** *The horizontal diameter of CAOC,* ***Dis-to-AB:*** *The distance between CAOC (the frontmost point) and the anterior boundary of the anterior skull base,* ***Dis-to-LB:*** *the distance between CAOC (the most lateral point) and the lateral boundary of the anterior skull base,* ***Dis-to-MSL:*** *The distance between CAOC (the most medial point) and the midsagittal line,* ***Ang-in-AP:*** *The angle between the optic canal and the sagittal horizontal line in axial plane,* ***Ang-in-SP:*** *The angle between the optic canal and the sagittal horizontal line in sagittal plane.*

Table V: Distribution of CAOC Shapes in CIM and the Control Group

Types	CIM	Control	Total	p-value
Tear-drop	42 (52.4%)	36 (45.0%)	78	0.423
Round	12 (15.0%)	20 (25.0%)	32	
Triangular	17 (21.3%)	14 (17.5%)	31	
Oval	9 (11.3%)	10 (12.5%)	19	
Total	80	80	160	

- The dispersion ratio of CAOC shapes relative to both groups is presented in Table V, which proves that the shape of the CAOC was not affected by the presence of a CIM ($p=0.423$).
- In both the groups, the CAOC-W was greater than the CAOC-H ($p<0.001$).

DISCUSSION

The downward herniation of the cerebellar tonsil into the foramen magnum is described as CIM (28). Its prevalence is approximately 0.24–3.6% (28). Its main cause is considered to be deviations in the development of the occipital somite, which originates from the paraxial mesoderm (5). The posterior fossa's bony components are considered the most affected structures in patients with CIM, who reportedly have a 23% smaller posterior fossa volume than the healthy controls (5, 51). The shrinking volume results in overcrowding of the hindbrain and causes various symptoms, such as vertigo, hearing loss, hoarseness, pain, facial numbness, and gait instability (5,38,51,54,58,59). Some authors claim that the entire skull, and not just the posterior fossa, is affected by CIM, possibly because of a mesodermal defect (52). The sphenoid sinus volume is reportedly 38% greater in patients with CIM than in healthy controls (9.3 ± 3.0 vs. 6.7 ± 1.9 cm^3; $p<0.001$) (39). Moreover, Patel et al. (45) encountered an enlarged pituitary gland on the radiological images of some patients with a Chiari type-II malformation (CIIM). Subsequently, they conducted a systematic investigation to examine the sella morphology on the magnetic resonance imaging (MRI) views of 21 patients. They observed that patients with CIIM had a taller pituitary gland (with no pathology), longer tuberculum sella, shorter dorsum sella, and shallow sella than healthy controls. The pituitary gland of patients with CIIM may appear slightly taller on MRI views because of the shallow sella. This may result in the normal gland being incorrectly interpreted as enlarged in such patients (45). These study results indicate that the angulation, size, and location of the anatomical structures around the sellar region (e.g., the optic canal) are significantly affected by CIM or CIIM.

Optic nerve compression may be seen in patients with CIM because of optic strut thickening and optic canal narrowing caused by pathological lesions such as osteopetrosis (4,20,37). Using an endoscopic transcaruncular approach, Medsinge et al. performed optic canal decompression in a pediatric patient (6-month-old girl) with CIM (37). The treatment procedures for optic canal compression are of great significance for surgeons (7,22,35,40,56,61,62). In some patients, 270° decompression is achieved by the removal of the optic strut and anterior clinoid process (7). In some patients, removal of only the optic canal's proximal portion, where compression most commonly occurs, is sufficient for decompression (22,56,62). Morphologic features of the structures around the sellar region may influence the selection of a suitable surgical procedure (8-10,22,24). For instance, if the position of the optic nerve is changed by a pathological entity distorting the optic canal, the safest way to avoid involuntary injury is to use the normal course of the optic nerve (24). An increase in the available anatomical data (results of surgical procedure investigations, quantitative assays, shape evaluations, and detailed morphologic definitions) regarding the structures (including the optic canal's proximal portion) around the sellar region may be helpful in reducing the morbidity and mortality rates (2,11,18,22,24,33,57). Our dataset focused on CT images of 40 patients with CIM with the aim to understand whether the optic canal of patients with CIM differs from that of normal individuals and determine whether procedures designed for normal individuals are appropriate for patients with CIM.

Our CAOC-H (CIM, 3.69 ± 0.69 mm; control, 3.75 ± 1.18 mm; p=0.243) and CAOC-W (CIM, 5.15 ± 0.96 mm; controls, 5.30 ± 1.25 mm; p=0.137) values were concordant with those of previous studies (Table VI) (1,3,12,21,25,29,32,34,46,47,49,50 ,53,57), in which the average CAOC-H was 3.60–5.17 mm and the average CAOC-W was 4.59–7.38 mm. Our findings indicate that CAOC-H and CAOC-W are not affected by CIM. In the CIM group, a significant difference was not observed between the right and left side values. However, in the control group, the left-sided measurements were greater than the right-sided measurements. Most previous studies have reported that there are no significant differences in measurements between the sides (1,11,25,46,47,49,57). However, Kalthur et al. observed a smaller left-sided opening (CAOC-H, 3.54 ± 0.71 mm; CAOC-W, 4.51 ± 0.79 mm) than the left-sided opening (CAOC-H, 3.67 ± 0.82 mm; CAOC-W, 4.68 ± 0.86 mm) (29). Kumar et al. also found a smaller CAOC-H on the left side than on the right side (32). However, we did not find a significant difference between males and females in the CIM group and the controls. Kalthur et al. observed smaller apertures in females (CAOC-H, 3.51 ± 0.82 mm; CAOC-W, 4.24 ± 0.67 mm) than in males (CAOC-H, 3.63 ± 0.74 mm; CAOC-W, 4.75 ± 0.83 mm) (29). Similarly, Ten et al. found smaller apertures in females (CAOC-H, 4.20 ± 0.60 mm; CAOC-W, 5.98 ± 0.86 mm) than in males (CAOC-H, 4.50 ± 0.64 mm; CAOC-W, 6.26 ± 0.80 mm) (57). However, Adanir et al. reported a similar CAOC-H in both sexes, but a smaller CAOC-W in females than in males (7 ± 1.09 vs. 7.54 ± 1.15 mm) (1).

In our study, the Ang-in-AP was greater in the CIM group than in the normal group (34.42° ± 5.29° vs. 31.80° ± 4.89°) (p=0.006). These findings were similar to those of previous articles (Table VII) (1,12,17,19,21,26,27,43,44,53,57,63), in which the average Ang-in-AP was 29.56–45.32°. Ten et al. observed a greater Ang-in-AP in the infancy period, and the angle did not change in the following periods. The Ang-in-SP was 15.04° ± 3.80° in patients with CIM and 14.97° ± 3.28° in healthy controls (p=0.598) (57). These values for both groups were similar to those of previous articles (Table VII) (1,17,43,57), in which the average Ang-in-SP was 7.57–18.20°. Ten et al. found a decrease in the Ang-in-SP with growth (infancy period, 24.87° ± 5.74° vs. postpubescence period, 12.81° ± 5.53°) (57). In both groups, there was no significant difference between the right and left sides, which was similar to findings of previous studies (1,57). In both groups, the Ang-in-AP was similar in both sexes. However, the Ang-in-SP was smaller in males than in females. Adanir et al. observed a smaller Ang-in-SP in females (7.24° ± 3.95°) than in males (7.89° ± 3.92°), and a similar Ang-in-AP in both sexes (1). However, Ten et al. did not find a significant difference in the angles between the sexes (57).

The Dis-to-MSL was 7.64 ± 1.64 mm in the CIM group and 7.67 ± 1.91 mm in the control group. This parameter was not affected by the presence of a CIM (p=0.982). Our study's Dis-to-MSL value was comparable to those of previous studies (Table VII) (1,17,25,43,57,63), in which the average Dis-to-MSL was 5.77–7.64 mm. Ten et al. observed an increase in the Dis-to-MSL with growth from the infancy period to the late childhood period (57). Thereafter, there was no subsequent change in the Dis-to-MSL. The Dis-to-LB was smaller in the CIM group than in the normal group (37.50 ± 4.21 vs. 37.50 ± 4.21 mm) (p=0.003). Our study's Dis-to-LB value was slightly smaller than that of previous studies (Table VI) (1, 57), in which the average Dis-to-LB was 41–42.55 mm. Ten et al. found an increase in the Dis-to-LB with growth from the infancy period to the early childhood period (57). Thereafter, there was no subsequent change in the Dis-to-LB. The Dis-to-AB was smaller in the CIM group than in the normal group (52.82 ± 6.14 vs. 57.41 ± 7.40 mm) (p<0.001). Our study's Dis-to-AB value was comparable to those of previous studies (Table VIII) (1,3,16,30,31,36,43,57), in which the average Dis-to-AB was 44.38–64.97 mm. In our opinion, the main reason for the wide range in Dis-to-AB and Dis-to-LB values was the selection of different landmarks. Ten et al. found an increase in the Dis-to-AB (i.e., the orbital depth) with growth from the infancy period to the postpubescence period (44.15 ± 2.51 vs. 58.20 ± 3.05 mm) (57). Our study findings demonstrated that the Dis-to-LB and Dis-to-AB were affected by the presence of a CIM. The short Dis-to-LB and Dis-to-AB may indicate that patients with CIM have a shorter and narrower anterior fossa than normal individuals. In the CIM and control groups, we did not find a significant difference between the left- and right-sided distance measurements, which is similar to the findings of

Table VI: Morphometric Data Related to the Dimension and Location of CAOC in the Literature

Study	Region	Specimen	n	Methods	CAOC-H (mm)	CAOC-W (mm)	Dis-to-LB (mm)
Akdemir et al. (3)	Türkiye	Adult dry skulls	50	Anatomic	-	R: 7.43 ± 1.95, L: 7.38 ± 2.01	-
Govsa et al. (21)	Türkiye	Dry skulls	318	Anatomic	R: 4.7 ± 0.79, L: 4.55 ± 0.65	R: 4.91 ± 0.49, L: 4.71 ± 0.43	-
Hart et al. (25)	USA	Adult patients	191	CT scans	4 (2-6)	6.7 (3-11)	-
Kalthur et al. (29)	India	Adult dry skulls	50	Anatomic	5.17 ± 0.81	5.48 ± 0.76	-
		Adult patients	214	CT scans	3.60 ± 0.76	4.59 ± 0.83	-
Berlis et al. (12)	Germany	Adult dry skulls	120	Anatomic	3.70 ± 0.60	6.25 ± 0.90	-
		Adult dry skulls	120	CT scans	3.63 ± 0.55	7.64 ± 1.11	-
Kumar et al. (32)	India	Adult dry skulls	60	Anatomic	R: 4.82 ± 0.77, L: 5.14 ± 0.73	R: 6.15 ± 0.81, L: 6 ± 0.86	-
Maniscalco and Habal (34)	USA	Cadavers	83	Anatomic	-	7.18 (5-9.5)	-
Prado et al. (46)	Brazil	Fetal dry skulls	50	Anatomic	-	R: 3.79 ± 0.65, L: 3.76 ± 0.66	-
		Child dry skulls	48	Anatomic	-	R: 4.67 ± 0.80, L: 4.72 ± 0.88	-
		Adult dry skulls	48	Anatomic	-	R: 5.24 ± 1.20, L: 5.43 ± 1.03	-
Purohit and Singh (47)	India	Adult dry skulls	300	Anatomic	-	R: 5.03 ± 0.72, L: 5.02 ± 0.76	-
Radunovic et al. (49)	Montenegro	Dry skulls	60	Anatomic	R: 4.65 ± 0.6, L: 4.55 ± 0.56	R: 4.90 ± 0.51, L: 4.85 ± 0.49	-
Rajeswaran et al. (50)	India	Dry skulls	140	Anatomic	-	R: 5.4, L: 5.5	-
Slavin et al. (53)	USA	Cadavers	40	Anatomic	-	5.14 ± 0.9	-
Beger (11)	Türkiye	Fetuses	50	Anatomic	1.58 ± 0.36	1.83 ± 0.59	-
Ten et al. (57)	Türkiye	Child Patients	400	CT scans	4.35 ± 0.64	6.12 ± 0.84	42.55 ± 3.28
Adanir et al. (1)	Türkiye	Adult Patients	800	CBCT	4.22 ± 0.74	7.27 ± 1.15	41.00 ± 4.05
This study	Türkiye	CIM	80	CT scans	3.69 ± 0.69	5.15 ± 0.96	37.50 ± 4.21
		Control	80	CT scans	3.75 ± 1.18	5.30 ± 1.25	39.43 ± 4.49

***n:** Numbers of sides, **CT:** Computed tomography, **CBCT:** Cone-beam computed tomography, **R:** Right, **L:** Left.*

previous studies (1,57). In the CIM group, these three distances were similar in both sexes. However, in the control group, the Dis-to-MSL was similar in both sexes, and the Dis-to-LB and Dis-to-AB were greater in males than in females. Similarly, Ten et al. and Adanir et al. determined that the Dis-to-LB and Dis-to-AB were greater in males than in females 1,57).

In the CIM group, the following four CAOC shapes were identified: teardrop (52.40%), triangular (21.30%), round (15%), and oval (11.30%). Similarly, in the control group, the following four CAOC shapes were identified: teardrop (45%), round (25%), triangular (17.50%), and oval (12.50%). Our study findings demonstrated that the CAOC shape was not affected by the presence of a CIM ($p = 0.423$). In previous studies (1,3,23,34,57), the seven different CAOC shapes were identified as follows: rhomboidal, oval (ovoid), elliptical, round, teardrop, triangular, and polygonal. In this study, elliptical-, rhomboidal-, and polygonal-shaped CAOCs were not identified. In previous studies (Table IX), the frequency of CAOC shapes was as follows: 11.8–100% for oval, 2.8–100% for round, 46.5–51.6% for teardrop, 22.5–39% for triangular, and

Table VII: Morphometric Data Related to the Angulation and Location of CAOC

Study	Regions	Specimens	n	Methods	Dis-to-MSL (mm)	Ang-in-AP (°)	Ang-in-SP (°)
Govsa et al. (21)	Türkiye	Dry skulls	318	Anatomic	R: 7.64 ± 1.18, L: 7.48 ± 2.01	R: 39.58 ± 4.03, L: 38.5 ± 3.27	-
Berlis et al. (12)	Germany	Adult dry skulls	120	CT scans	-	39.1	-
Harwood-Nash (26)	Canada	Children	150	CT scans	-	39.5	-
Slavin et al. (53)	USA	Cadavers	40	Anatomic	-	29.56 (22-34)	-
Öztürk et al. (43)	Türkiye	Adult dry skulls	152	Anatomic	R: 6.8, l: 6.9	R: 38.8, L: 38.1	R: 16.9, L: 18.2
Park et al. (44)	Korea	Patients	50	CT scans	-	39.9±4.63	-
Cheng et al. (17)	China	Patients	400	CT scans	R: 6.64 ± 0.97, L: 6.48 ± 0.90	R: 45.32 ± 4.67, L: 44.21 ± 4.46	R: 10.27 ± 5.79, L: 10.34 ± 6.17
Hayashi et al. (27)	Japan	Adult cadavers	39	Anatomic	-	41.8 (28-51)	-
Zhang et al. (63)	China	Adult patients	240	CT scans	R: 7.01 ± 1.43, L: 6.99 ± 1.28	43.23 ± 4.47	-
Goldberg et al. (19)	USA	Cadavers	4	Radioanatomic	-	30	-
Ten et al. (57)	Türkiye	Child Patients	400	CT scans	7.17 ± 1.48	39.28 ± 5.13	16.01 ± 6.76
Adanir et al. (1)	Türkiye	Adult Patients	800	CBCT scans	5.77 ± 1.32	38.96 ± 4.36	7.57 ± 3.95
This study	Türkiye	CIM	80	CT scans	7.64 ± 1.64	34.42 ± 5.29	15.04 ± 3.80
		Control	80	CT scans	7.67 ± 1.91	31.80 ± 4.89	14.97 ± 3.28

***n:** Numbers of sides, **CT:** Computed tomography, **CBCT:** Cone-beam computed tomography.*

Table VIII: Morphometric Data Related to Dis-to-AB in the Literature

Studies	Specimen	n	Methods	Landmark points	Landmark points	Measurements
Akdemir et al. (3)	Adult dry skulls	50	Anatomic	Frontal-maxilla-lacrimal conjunction	CAOC	R: 49.52 ± 2.62, L: 50.94 ± 3.35
Öztürk et al. (43)	Adult dry skulls	152	Anatomic	Anterior border of ACF	Limbus sphenoidale	44.5 (34.2-53.7)
Karampatakis et al. (30)	Dry skulls	50	Anatomic	Inferior orbital rim	Lateral margin of CAOC	49.62 ± 2.46
Cheng et al. (16)	Dry skulls	194	Anatomic	Inferior orbital rim	Optic canal	44.38 ± 3.55
Katsev et al. (31)	Adult dry skulls	120	Anatomic	Inferior temporal orbital rim	Nasal entrance of optic foramen	42-54
McQueen et al. (36)	Cadavers	54	Anatomic	Intraorbital foramen	Optic canal	49.73 ± 2.71
				Supraorbital foramen or notch	Optic canal	48.65 ± 3.21
Ten et al. (57)	Child Patients	400	CT scans	Anterior boundary of ACF	Anterior rim of CAOC	54.04 ± 5.23
Adanir et al. (1)	Adult Patients	800	CBCT scans	Anterior boundary of ACF	Anterior rim of CAOC	64.97 ± 6.36
This study	CIM	80	CT scans	Anterior boundary of ACF	Anterior rim of CAOC	52.82 ± 6.14
	Control	80	CT scans	Anterior boundary of ACF	Anterior rim of CAOC	57.41 ± 7.40

***ACF:** Anterior cranial fossa, **CT:** Computed tomography, **CBCT:** Cone-beam computed tomography.*

Table IX: Literature Data Related to CAOC Shape

Studies	Region	n	Methods	Sample	Elliptical	Oval (Ovoid)	Round	Tear-drop	Triangular	Rhomboidal	Polygonal
Akdemir et al. (3)	Türkiye	50	Anatomic	Adult dry skulls	100%	-	-	-	-	-	-
Maniscalco and Habal (34)	USA	83	Anatomic	Cadavers	100%	-	-	-	-	-	-
Govsa et al. (21)	Türkiye	318	Anatomic	Dry skulls	-	100%	-	-	-	-	-
Purohit and Singh (47)	India	300	Anatomic	Dry skulls	-	100%	-	-	-	-	-
Kumar et al. (32)	India	60	Anatomic	Dry skulls	-	-	100%	-	-	-	-
Slavin et al. (53)	USA	40	Anatomic	Cadavers	-	-	100%	-	-	-	-
Guseva and Denisov (23)	Belarus	469	Radioanatomic	-	-	+	+	-	+	+	+
Beger (11)	Türkiye	50	Anatomic	Fetal cadavers	-	72%	28%	-	-	-	-
Ten et al. (57)	Türkiye	400	CT scans	Child patients	-	11.8%	2.8%	46.5%	39%	-	-
Adanir et al. (1)	Türkiye	800	CBCT scans	Adult patients	-	19.8%	3.8%	51.6%	22.5%	-	2.4%
This study	Türkiye	80	CT scans	CIM	-	11.3%	15%	52.4%	21.3%	-	-
		80	CT scans	Control	-	12.5%	25%	45%	17.5%	-	-

***n:** Number of sides, **CT:** Computed tomography, **CBCT:** Cone-beam computed tomography, **+:** The findings without percentages.*

2.4% for polygonal. These rates demonstrate that shape definitions are quite variable. The main reasons for the variations between works may be regional differences, small-scale studies, and imperfect techniques (21,23,34,47,57).

Recent studies have demonstrated that not only the bony components of the posterior fossa but also those of the anterior and middle fossae are affected by CIM. Ozalp et al. reported that patients with CIM had a shorter anterior clinoid process, longer optic strut, more anteriorly located optic strut, wider angled anterior clinoid process, and greater sulcal angle (angle between the prechiasmatic sulcus and sphenoidal yoke) than healthy controls (41,42). Nwotchouang et al. observed that the ST area in patients with CIM was 27% smaller than that in normal individuals (69.7 ± 22.1 vs. 95.1 ± 23.8 mm^2, p<0.001) (39). Bas et al. found a smaller sella volume in patients with CIM than in healthy controls (41.4 vs. 53.3 mm^3, p=0.034) (6). In this study, we determined that patients with CIM have a greater Ang-in-AP, shorter Dis-to-LB, and shorter Dis-to-AB than normal individuals.

CONCLUSION

In this study, we observed a shorter Dis-to-AB, greater Ang-in-AP, and shorter Dis-to-LB in patients with CIM than in healthy individuals. The shorter Dis-to-AB and Dis-to-LB demonstrate that patients with CIM have a shorter and narrower anterior fossa than normal individuals. Furthermore, the distribution rate of the CAOC shape relative to both groups demonstrated that the aperture shape was not affected by the presence of a CIM. Thus, Dis-to-AB and Dis-to-LB should be evaluated in patients with CIM during preoperative radiologic examinations to ensure safe performance of optic canal decompression.

Declarations

Funding: This research did not receive any specific grant from funding agencies in the public, commercial, or not-for-profit sectors.

Availability of data and materials: Available with the author on request.

Disclosure: The authors declare no conflict of interest.

AUTHORSHIP CONTRIBUTION

Study conception and design: HO, OO, BCA, OB
Data collection: AI, SO, EA, HU, BCA
Analysis and interpretation of results: AI, SO, EA, OB
Draft manuscript preparation: OB, BCA, SO, HU
Critical revision of the article: BCA, OB, OO, HO, EA
All authors (HO, OO, BCA, EA, AI, HU, SO, OB) reviewed the results and approved the final version of the manuscript.

REFERENCES

1. Adanir SS, Baksi YE, Beger O, Bahsi I, Kervancioglu P, Yalcin ED, Orhan M: Evaluation of the cranial Aperture of the optic canal on cone-beam computed tomography images and its clinical Implications for the transcranial approaches. J Craniofac Surg 33:1909-1913, 2022. https://doi.org/10.1097/SCS.0000000000008577
2. Adanir SS, Beger O, Bahsi I: A terminological confusion: Optic foramen or canal? Surg Radiol Anat 43:577-578, 2021. https://doi.org/10.1007/s00276-021-02679-9
3. Akdemir G, Tekdemir I, Altin L: Transethmoidal approach to the optic canal: surgical and radiological microanatomy. Surg Neurol 62:268-274, 2004. https://doi.org/10.1016/j.surneu.2004.01.022
4. Alagappan A, Satpathy AK, Sahoo B, Nayak MK: Osteopetrosis with Arnold Chiari malformation type I. BMJ Case Rep 16:e254559, 2023. https://doi.org/10.1136/bcr-2023-254559
5. Aydin S, Hanimoglu H, Tanriverdi T, Yentur E, Kaynar MY: Chiari type I malformations in adults: A morphometric analysis of the posterior cranial fossa. Surg Neurol 64:237-241, 2005. https://doi.org/10.1016/j.surneu.2005.02.021
6. Bas G, Ozkara E, Ozbek Z, Naderi S, Arslantas A: Sella volume and posterior fossa morphometric measurements in Chiari type 1. Turk Neurosurg 33:290-295, 2023. https://doi.org/10.5137/1019-5149.JTN.40088-22.4
7. Beer-Furlan A, Evins AI, Rigante L, Burrell JC, Anichini G, Stieg PE, Bernardo A: Endoscopic extradural anterior clinoidectomy and optic nerve decompression through a pterional port. J Clin Neurosci 21:836-840, 2014. https://doi.org/10.1016/j.jocn.2013.10.006
11. Beger O: Assessment of the optic foramen shape and size in human fetuses. J Craniofac Surg 31:2021-2024, 2020. https://doi.org/10.1097/SCS.0000000000006610
8. Beger O, Bahsi I: Chiasmatic Ridge: incidence, classification, and clinical implications. J Craniofac Surg 32:1910-1912, 2021. https://doi.org/10.1097/SCS.0000000000007291
9. Beger O, Taghipour P, Cakir S, Hamzaoglu V, Ozalp H, Kara E, Vayisoglu Y, Dagtekin O, Dagtekin A, Bagdatoglu C, Ozturk AH, Talas DU: Fetal anatomy of the optic strut and prechiasmatic sulcus with a clinical perspective. World Neurosurg 136:e625-e634, 2020. https://doi.org/10.1016/j.wneu.2020.01.125
10. Beger O, Ten B, Balci Y, Cakir S, Ozalp H, Hamzaoglu V, Vayisoglu Y, Dagtekin A, Bagdatoglu C, Talas DU: A computed tomography study of the prechiasmatic sulcus anatomy in children. World Neurosurg 141:e118-e132, 2020. https://doi.org/10.1016/j.wneu.2020.05.023
12. Berlis A, Putz R, Schumacher M: Direct and CT measurements of canals and foramina of the skull base. Brit J Radiol 65:653-661, 1992. https://doi.org/10.1259/0007-1285-65-776-653
13. Caporlingua A, Prior A, Cavagnaro MJ, Winston G, Oliveira DLC, Sadwhani SD, Arias GA, Schwalb JN, Akhbari M, Evins AI, Bernardo A: The intracranial and intracanalicular optic nerve as seen through different surgical windows: Endoscopic versus transcranial. World Neurosurg 124:522-538, 2019. https://doi.org/10.1016/j.wneu.2019.01.122
14. Cares H, Bakay L: The clinical significance of the optic strut. J Neurosurg 34:355-364, 1971. https://doi.org/10.3171/jns.1971.34.3.0355
15. Chang JT, Morrison CS, Styczynski JR, Mehan W, Sullivan SR, Taylor HO: Pediatric orbital depth and growth: A radiographic analysis. J Craniofac Surg 26:1988-1991, 2015. https://doi.org/10.1097/SCS.0000000000001974
16. Cheng A, Lucas P, Yuen H, Lam D, So K: Surgical anatomy of the Chinese orbit. Ophthalmic Plast Reconstr Surg 24:136-141, 2008. https://doi.org/10.1097/IOP.0b013e31816704f5
17. Cheng Y, Liu M, Zhang S, Tian Y, Song D, Li Y, Luo Q: Optic canal (OC) and internal carotid artery (ICA) in sellar region. Surg Radiol Anat 35:797-801, 2013. https://doi.org/10.1007/s00276-013-1193-2
18. Gagliardi F, Donofrio CA, Spina A, Bailo M, Gragnaniello C, Gallotti AL, Elbabaa SK, Caputy AJ, Mortini P: Endoscope-assisted transmaxillosphenoidal approach to the sellar and parasellar regions: An anatomic study. World Neurosurg 95:246-252, 2016. https://doi.org/10.1016/j.wneu.2016.08.034
19. Goldberg RA, Hannani K, Toga AW: Microanatomy of the orbital apex: Computed tomography and microcryoplaning of soft and hard tissue. Ophthalmology 99:1447-1452, 1992. https://doi.org/10.1016/S0161-6420(92)31785-3
20. Goodwin D, Halvorson AR: Chiari I malformation presenting as downbeat nystagmus: Clinical presentation, diagnosis, and management. Optometry 83:80-86, 2012
21. Govsa F, Erturk M, Kayalioglu G, Pinar Y, Ozer M, Ozgur T: Neuro-arterial relations in the region of the optic canal. Surg Radiol Anat 21:329-335, 1999. https://doi.org/10.1007/BF01631334
22. Guler TM, Yilmazlar S, Ozgun G: Anatomical aspects of optic nerve decompression in transcranial and transsphenoidal approach. J Craniomaxillofac 47:561-569, 2019. https://doi.org/10.1016/j.jcms.2019.01.027
23. Guseva Y, Denisov S: Structure of the optic canal in human ontogenesis. Ann Anat 188:103-116, 2006. https://doi.org/10.1016/j.aanat.2005.05.007
24. Guthikonda B, Tobler WD Jr, Froelich SC, Leach JL, Zimmer LA, Theodosopoulos PV, Tew JM Jr, Keller JT: Anatomic study of the prechiasmatic sulcus and its surgical implications. Clin Anat 23:622-628, 2010. https://doi.org/10.1002/ca.21002
25. Hart CK, Theodosopoulos PV, Zimmer LA: Anatomy of the optic canal: A computed tomography study of endoscopic nerve decompression. Ann Otol Rhinol Laryngol 118:839-844, 2009. https://doi.org/10.1177/000348940911801203
26. Harwood-Nash D: Axial tomography of the optic canals in children. Radiology 96:367-374, 1970. https://doi.org/10.1148/96.2.367
27. Hayashi N, Masuoka T, Tomita T, Sato H, Ohtani O, Endo S: Surgical anatomy and efficient modification of procedures for selective extradural anterior clinoidectomy. Minim Invasive Neurosurg 47:355-358, 2004. https://doi.org/10.1055/s-2004-830121
28. Kahn EN, Muraszko KM, Maher CO: Prevalence of Chiari I malformation and syringomyelia. Neurosurg Clin N Am 26:501-507, 2015. https://doi.org/10.1016/j.nec.2015.06.006

29. Kalthur S, Periyasamy R, Kumar S, Gupta C, D'souza AS: A morphometric evaluation of the optic canal: Comparative study between computerized tomographic study and direct anatomic study. Saudi J Med Med Sci 3:204-208, 2015. https://doi.org/10.4103/1658-631X.161997
30. Karampatakis V, Natsis K, Gigis P, Stangos N: Orbital depth measurements of human skulls in relation to retrobulbar anesthesia. Eur J Ophthalmol 8:118-120, 1998. https://doi.org/10.1177/112067219800800212
31. Katsev DA, Drews RC, Rose BT: An anatomic study of retrobulbar needle path length. Ophthalmology 96:1221-1224, 1989. https://doi.org/10.1016/S0161-6420(89)32748-5
32. Kumar A, Tripathi A, Jain S, Khare S, Kaushik RK, Kausar H, Arora S: Anatomical and morphometric study of optic foramen in North Indian Population. Natl J Clin Anat 8:053-056, 2019. https://doi.org/10.1055/s-0039-1689079
33. Locatelli M, Di Cristofori A, Draghi R, Bertani G, Guastella C, Pignataro L, Mantovani G, Rampini P, Carrabba G: Is complex sphenoidal sinus anatomy a contraindication to a transsphenoidal approach for resection of sellar lesions? Case series and review of the literature. World Neurosurg 100:173-179, 2017. https://doi.org/10.1016/j.wneu.2016.12.123
34. Maniscalco JE, Habal MB: Microanatomy of the optic canal. J Neurosurg 48:402-406, 1978. https://doi.org/10.3171/jns.1978.48.3.0402
35. Maurer J, Hinni M, Mann W, Pfeiffer N: Optic nerve decompression in trauma and tumor patients. Eur Arch Otorhinolaryngol 256:341-345, 1999. https://doi.org/10.1007/s004050050160
36. Mcqueen CT, Diruggiero DC, Campbell JP, Shockley WW: Orbital osteology: A study of the surgical landmarks. Laryngoscope 105:783-788, 1995. https://doi.org/10.1288/00005537-199508000-00003
37. Medsinge A, Sylvester C, Tyler-Kabara E, Stefko ST: Bilateral endoscopic optic nerve decompression in an infant with osteopetrosis. J AAPOS 23:40-42, 2019. https://doi.org/10.1016/j.jaapos.2018.05.012
38. Nishikawa M, Sakamoto H, Hakuba A, Nakanishi N, Inoue Y: Pathogenesis of Chiari malformation: A morphometric study of the posterior cranial fossa. J Neurosurg 86:40-47, 1997. https://doi.org/10.3171/jns.1997.86.1.0040
39. Nwotchouang BST, Eppelheimer MS, Bishop P, Biswas D, Andronowski JM, Bapuraj JR, Frim D, Labuda R, Amini R, Loth F: Three-dimensional CT morphometric image analysis of the clivus and sphenoid sinus in Chiari malformation type I. Ann Biomed Eng 47:2284-2295, 2019. https://doi.org/10.1007/s10439-019-02301-5
40. Onofrey CB, Tse DT, Johnson TE, Neff AG, Dubovy S, Buck BE, Casiano R: Optic canal decompression: A cadaveric study of the effects of surgery. Ophthalmic Plast Reconstr Surg 23:261-266, 2007. https://doi.org/10.1097/IOP.0b013e3180cac220
41. Ozalp H, Ozgural O, Alpergin BC, Inceoglu A, Ozalp S, Armagan E, Ucar H, Beger O: Analysis of the prechiasmatic sulcus in Chiari malformation type I. World Neurosurg 175:e1149-e1157, 2023. https://doi.org/10.1016/j.wneu.2023.04.083
42. Ozalp H, Ozgural O, Alpergin BC, Inceoglu A, Ozalp S, Armagan E, Ucar H, Beger O: Assessment of the anterior clinoid process and optic strut in Chiari malformation type I: A computed tomography study. J Neurol Surg B Skull Base 85:302-312, 2023. doi.org/10.1055/s-0043-57248, 2023. https://doi.org/10.1055/s-0043-57248
43. Ozturk A, Bozbuga M, Bayraktar B, Ari Z, Sahinoglu K, Polat G, Gurel I: Surgical anatomy and morphometric analysis of the optico-chiasmatic apparatus, optic canal and sphenoid ridge. Okajimas Folia Anat Jpn 75:319-322, 1999. https://doi.org/10.2535/ofaj1936.75.6_319
44. Park SJ, Yoo JN, Yoo MS, Heo YC: A study on double angle of optic foramen in the Rhese method. J Korean Soc Radiol 11:313-319, 2017
45. Patel D, Saindane A, Oyesiku N, Hu R: Variant sella morphology and pituitary gland height in adult patients with Chiari II malformation: Potential pitfall in MRI evaluation. Clin Imaging 64:24-28, 2020. https://doi.org/10.1016/j.clinimag.2020.02.014
46. Prado PA, Ribeiro EC, De Angelis MA, Smith RL: Biometric study of the optic canal during cranial development. Orbit 26:107-111, 2007. https://doi.org/10.1080/01676830600987540
47. Purohit BJ, Singh PR: An osteologic study of cranial opening of optic canal in Gujarat region. J Clin Diagn Res 10:AC08-AC11, 2016. https://doi.org/10.7860/JCDR/2016/22110.8929
48. Puzzilli F, Ruggeri A, Mastronardi L, Agrillo A, Ferrante L: Anterior clinoidal meningiomas: Report of a series of 33 patients operated on through the pterional approach. Neuro Oncol 1:188-195, 1999. https://doi.org/10.1215/S1522851798000210
49. Radunovic M, Vukcevic B, Radojevic N, Vukcevic N, Popovic N, Vuksanovic-Bozaric A: Morphometric characteristics of the optic canal and the optic nerve. Folia Morphol (Warsz) 78:39-46, 2019
50. Rajeswaran SA, Mohanraj KG, Babu KY: An osteologic study of the cranial opening of optic canal in dry human skulls. Drug Invent Today 12:251-253, 2019
51. Schady W, Metcalfe RA, Butler P: The incidence of craniocervical bony anomalies in the adult Chiari malformation. J Neurol Sci 82:193-203, 1987. https://doi.org/10.1016/0022-510X(87)90018-9
52. Sgouros S, Kountouri M, Natarajan K: Skull base growth in children with Chiari malformation Type I. J Neurosurg 107:188-192, 2007. https://doi.org/10.3171/PED-07/09/188
53. Slavin KV, Dujovny M, Soeira G, Ausman JI: Optic canal: Microanatomic study. Skull Base Surg 4:136-144, 1194. https://doi.org/10.1055/s-2008-1058965
54. Sperling NM, Franco RA Jr, Milhorat TH: Otologic manifestations of Chiari I malformation. Otol Neurotol 22:678-681, 2001. https://doi.org/10.1097/00129492-200109000-00020
55. Standring S, Borley N, Collins P, Crossman A, Gatzoulis M, Healy J: Gray's Anatomy: The Anatomical Basis of Clinical Practice, 41st ed. London: Elsevier, 2008:667-668

56. Taha AN, Erkmen K, Dunn IF, Pravdenkova S, Al-Mefty O: Meningiomas involving the optic canal: pattern of involvement and implications for surgical technique. Neurosurg Focus 30:E12, 2011. https://doi.org/10.3171/2011.2.FOCUS1118
57. Ten B, Beger O, Esen K, Adanir SS, Hamzaoglu EC, Cicek F, Taghipour P, Kara E, Vayisoglu Y, Talas DU: Anatomic features of the cranial aperture of the optic canal in children: A radiologic study. Surg Radiol Anat 43:187-199, 2021. https://doi.org/10.1007/s00276-020-02604-6
58. Trigylidas T, Baronia B, Vassilyadi M, Ventureyra EC: Posterior fossa dimension and volume estimates in pediatric patients with Chiari I malformations. Childs Nerv Syst 24:329-336, 2008. https://doi.org/10.1007/s00381-007-0432-4
59. Tubbs RS, McGirt MJ, Oakes WJ: Surgical experience in 130 pediatric patients with Chiari I malformations. J Neurosurg 99:291-296, 2003. https://doi.org/10.3171/jns.2003.99.2.0291
60. Vohra ST, Escott EJ, Stevens D, Branstetter BF: Categorization and characterization of lesions of the orbital apex. Neuroradiology 53:89-107, 2011. https://doi.org/10.1007/s00234-010-0712-7
61. Yang Y, Wang H, Shao Y, Wei Z, Zhu S, Wang J: Extradural anterior clinoidectomy as an alternative approach for optic nerve decompression: Anatomic study and clinical experience. Neurosurgery 59:ONS253-262; discussion ONS262, 2006. https://doi.org/10.1227/01.NEU.0000236122.28434.13
62. Yilmazlar S, Saraydaroglu O, Korfali E: Anatomical aspects in the transsphenoidal-transethmoidal approach to the optic canal: An anatomic-cadaveric study. J Craniomaxillofac Surg 40:e198-e205, 2012. https://doi.org/10.1016/j.jcms.2011.10.008
63. Zhang H, Liu X, Cheng Y, Zhang S, Wang C, Cui D, Li Y, Fu Y, Wang Y: A new method of locating the optic canal based on structures in sella region: Computed tomography study. J Craniofac Surg 24:1011-1015, 2013. https://doi.org/10.1097/SCS.0b013e318287d228